Journal of Green Chemical and Environmental Engineering

e-ISSN 3090-2568
p-ISSN 3109-2233
Research Paper

Sustainable Conversion of Palm Kernel Shells into Activated Carbon for the Removal of Cu^{2+} and Zn^{2+} from Industrial Paint Wastewater

Opeoluwa Damilola Sole-Adeoye[1,*], Idayat Adebukola Olowonyo[1], Kazeem Kolapo Salam[2], Oreofe Toyin Adedayo[3], Odunayo Deborah Akinwumi[2], Stephen Omoniyi Owolabi[1]

[1]*Department of Chemical Engineering, Faculty of Engineering, Adeleke University, Ogbomoso, Oyo, State, Nigeria.*
[2]*Department of Chemical Engineering, Faculty of Engineering, Ede Ladoke Akintola University of Technology, Osun state Nigeria.*
[3]*Department of Chemical Engineering, College of Engineering, Landmark University, Omu aran, Kwara State, Nigeria*

** Corresponding author: soleadeoye.opeoluwa@adelekeuniversity.edu.ng (Opeoluwa Damilola Sole-Adeoye)*

Received 8 July 2025
Revised 27 Sept 2025
Accepted 30 Sept 2025

Citation: D. Sole-Adeoye Opeoluwa D, A. Olowonyo Idayat, K. Salam Kazeem. (2025). "Sustainable Conversion of Palm Kernel Shells into Activated Carbon for the Removal of Cu^{2+} and Zn^{2+} from Industrial Paint Wastewater". J. of Green Chemical and Environmental Engineering, Vol. 1, No. 3, 169-183.

: 10.63288/jgcee.v1i3.14

Abstract: Industrial paint effluents are major contributors to aquatic heavy metal contamination, creating serious environmental and public health concerns. Conventional treatment methods are often costly and unsustainable, underscoring the need for renewable and effective alternatives. In this study, palm kernel shells (PKS), an abundant agricultural byproduct, were valorized into activated carbon (PKS-AC) for the removal of Cu^{2+} and Zn^{2+} ions from real paint effluent. The adsorbent was prepared through chemical activation and high-temperature carbonization, yielding a material with high fixed carbon content (69.2%) and reduced volatile matter (14.0%), which provided structural stability and enhanced adsorption sites. Batch adsorption experiments revealed optimal conditions at pH 7, 90 minutes, 2.0 g/L dosage, and 55 °C, achieving removal efficiencies of 68.75% (Cu^{2+}) and 67.50% (Zn^{2+}). Kinetic modeling followed the pseudo-second-order model, suggesting chemisorption, while thermodynamic analysis confirmed the process to be spontaneous and endothermic. Importantly, regeneration tests showed PKS-AC retained strong performance over multiple cycles, highlighting its reusability. The novelty of this work lies in demonstrating the efficacy of PKS-derived activated carbon for treating real industrial paint wastewater, rather than synthetic solutions, while providing a complete evaluation of adsorption performance, kinetics, thermodynamics, and reusability. These findings establish PKS-AC as a sustainable, cost-effective, and circular-economy-driven adsorbent for large-scale wastewater treatment.

Keywords: Activated carbon; Palm kernel shell; Paint effluent; Copper; Zinc; Waste valorization.

1. Introduction

Heavy metal contamination in surface and groundwater continues to pose significant environmental and health challenges, particularly in industrial zones where untreated effluents are frequently discharged. Among various pollutants, cadmium (Cd^{2+}), copper (Cu^{2+}), lead (Pb^{2+}), and zinc (Zn^{2+}) are of particular concern due to their toxicity, persistence, and ability to bioaccumulate within living organisms [1], [2]. Paint manufacturing industries contribute substantially to heavy metal

discharge through the release of colorants, stabilizers, and corrosion inhibitors that contain these elements [3]. Their wastewater often contains heavy metals (Cu^{2+}, Zn^{2+}, Pb^{2+}, Cd^{2+}, Cr^{6+}), organic solvents, binders, surfactants, suspended solids, and has variable pH and high COD, which makes treatment highly challenging [4]. Chronic exposure to Cu^{2+} and Zn^{2+}, even at low concentrations, has been associated with adverse effects such as kidney damage, liver damage, neurological disorders, and disruptions in plant and microbial growth [5], [6]. As such, effective elimination of these metals from industrial wastewater is imperative to safeguard both human and environmental health.

Conventional technologies used for eliminating heavy metals from industrial wastewater, including chemical precipitation, ion exchange, electrocoagulation, and membrane-based filtration, are often associated with high operational costs, limited selectivity, and generation of toxic sludge [7], [8]. Consequently, there has been growing interest in low-cost and sustainable alternatives for wastewater treatment. Among such methods, adsorption using carbonaceous materials has emerged as an effective and economically viable technique due to its simplicity, adaptability, and high removal efficiencies.

Activated carbon derived from lignocellulosic agricultural wastes has gained significant attention due to its abundant availability, low cost, and favourable textural and chemical properties. Biomass precursors such as coconut shells, rice husks, and sawdust have been widely investigated. However, palm kernel shells (PKS), a byproduct from palm oil processing, remain largely underutilized despite their high fixed carbon content and porous structure [9], [10]. The open burning or indiscriminate disposal of PKS contributes to environmental degradation, but its conversion into activated carbon provides an avenue for both waste valorization and pollution control.

The novelty of this research lies in the valorization of PKS into NaOH-assisted activated carbon for the removal of Cu^{2+} and Zn^{2+} from real paint industry effluent. Unlike previous studies that used synthetic solutions or other biomass precursors, this work demonstrates the dual removal of metals from actual industrial wastewater, combined with adsorption modelling and FTIR characterization to elucidate the interaction mechanisms. This study is among the few to employ palm kernel shell-derived activated carbon (PKS-AC) for the treatment of *real paint effluent* rather than synthetic metal solutions. The research combines adsorption performance with kinetic, thermodynamic, and regeneration analyses, thereby demonstrating both the mechanistic insights and practical reusability of PKS-AC as a sustainable adsorbent for industrial wastewater treatment

2. Research and Methodology

2.1. Materials and Reagents

Palm kernel shells (PKS) were sourced from a palm oil processing facility in Ede, Osun State, Nigeria. The raw biomass was thoroughly rinsed with distilled water to eliminate residual oil, dirt, and particulates, then air-dried and stored in airtight containers until use. All chemicals used, namely sodium hydroxide (NaOH), hydrochloric acid (HCl) and nitric acid (HNO_3), were of analytical grade and sourced from Sigma-Aldrich, Germany. Double-distilled water (produced using a Thermo Scientific™ Barnstead™ Smart2Pure system, USA) was utilized for all solution preparations. Laboratory glassware (Pyrex™, USA) included 250 mL conical flasks, beakers, a 100 mL measuring cylinder, and funnels.

2.2. Preparation of Palm Kernel Shell-Based Activated Carbon

The collected PKS feedstock was first oven-dried at 70°C for 48 hours using a Memmert UN55 Universal Oven, Germany to remove moisture [12]. After drying, the PKS samples were crushed to increase surface area and sieved (Endecotts Sieve Shaker, UK) to obtain particles within the 1–2 mm size range. Chemical activation was carried out by soaking the sieved PKS in 0.5 M NaOH solution

(1:1 w/w) for 24 hours under ambient conditions. After filtration, the pre-treated PKS was dried at 100°C for 4 hours, then carbonized in a muffle furnace (Carbolite CWF 1200, UK) at 600°C for one hour. After carbonization, the sample was cooled in a desiccator (Duran, Germany). The PKS-derived activated carbon (PKS-AC) was thoroughly washed with distilled water until a neutral pH was achieved and then oven-dried at 110°C for 2 hours before storage.

2.3. Effluent Sampling and Characterization

Wastewater samples were collected from a paint manufacturing facility in Osun State, Nigeria, and preserved at 4 °C prior to use. On-site measurements of pH were conducted using a calibrated digital pH meter (Hanna Instruments, model HI2211). For batch adsorption studies, pH values were adjusted using 0.1 M HCl or 0.1 M NaOH as required. Cu^{2+} and Zn^{2+} concentrations were quantified using a UV–Visible spectrophotometer (Spectrum Lab 7525) at 340 nm and 351 nm, respectively, based on calibration curves prepared from standard solutions.

2.4. Characterization of the Synthesized Adsorbent

Standard ASTM procedures were used to evaluate proximate composition, including moisture content, volatile components, ash residue, and fixed carbon percentage [13]. Metal ion concentrations before and after adsorption were determined using Atomic Absorption Spectrophotometry (AAS, Shimadzu AA-7000, Japan).).

2.4.1. Moisture Content Determination

A 2 g sample was weighed into a crucible, and the initial combined weight was recorded as W_1. PKS-AC was then heated in an oven at 100°C for one hour, cooled, reweighed, and heated further until constant weight was achieved, following Onwukeme and Egemba [13].

$$\%\ Moisture\ content = \frac{W_1 - W_2}{W_1} \times 100 \quad (1)$$

Where, $W_1 = weight\ of\ crucible\ and\ sample\ before\ drying$,
$W_2 = weight\ of\ crucible\ and\ sample\ after\ drying$

2.4.2 Ash Content

2 g of PKS-AC was weighed into a crucible. The initial weight including the crucible was recorded as W_2. The sample was placed inside a muffle furnace at 500°C for three hours, cooled, and reweighed as W_3.

$$\%\ Ash\ content = \frac{W_3 - W_1}{W_2 - W_1} \times 100 \quad (2)$$

Where, $W_1 = weight\ of\ empty\ crucible$, $W_2 = weight\ of\ crucible\ and\ sample\ before\ heating$, $W_3 = weight\ of\ crucible\ and\ sample\ after\ heating (ash)$

2.4.3. Volatile Matter Content

The determination of volatile matter (VM) content followed the method described by Ekpete *et al*. [8]. A 1 g sample was placed in a crucible, covered, and heated at 500°C for 10 minutes. Mass loss was recorded as volatile matter content.

$$V_m = \frac{(w_d - w_h)}{w_d} \times 100 \quad (3)$$

2.4.4. Fixed Carbon Estimation

The fixed carbon content was determined by deducting the combined percentages of moisture, subtracting the sum of volatile matter, and ash content from a total of 100%, as given in Equation (4):

$$\%Fixed\ carbon = 100 - (VM\ + MC + +AC) \quad (4)$$

2.4.5. Bulk Density Determination

Bulk density was measured by gently filling a known volume of adsorbent into a measuring cylinder, tapping gently, and recording mass and volume:

$$\text{Bulk Density (g/cm}^3\text{)} = \text{Mass / Volume} \quad (5)$$

2.4.6 Fourier Transform Infrared Spectroscopy (FTIR)

FTIR spectra of PKS-AC were recorded using a PerkinElmer Spectrum 100 spectrometer (USA) in the range of 4000–400 cm^{-1} with 4 cm^{-1} resolution and 32 scans per sample. Functional groups before and after metal ion adsorption were compared, focusing on shifts in peak positions (e.g., –OH, C=O, C–O–C). A decrease in peak intensity or a shift in wavenumber was taken as evidence of metal–functional group interactions during adsorption.

2.5. Calibration and Standard Solutions

Stock solutions of Cu^{2+} and Zn^{2+} (1000 mg/L) were prepared and diluted to 50–200 mg/L working standards. A UV-Vis spectrophotometer determined λmax values (340 nm for Cu^{2+}, 351 nm for Zn^{2+}). Calibration curves were generated and equilibrium concentrations determined from the regression equation in equation (6):

$$C_e\left({}^{mg}/_{L}\right) = \frac{y - C}{M} \quad (6)$$

where y = absorbance, C = intercept, M = slope.

2.6. Batch Adsorption Studies

Batch adsorption experiments assessed the effectiveness of PKS-derived activated carbon in removing Cu^{2+} and Zn^{2+} under varying conditions of pH (2–12), adsorbent dosage (0.5–2.5 g/L), contact time (30–120 min), and temperature (25–55°C). A fixed 10 mL volume of paint effluent was treated with PKS-AC under constant shaking at 150 rpm. The pH of the effluent was measured using a calibrated digital pH meter (Hanna Instruments, model HI 2211), and adjusted using 0.1 M HCl or 0.1 M NaOH solutions as required. Post-treatment samples were filtered, and metal concentrations measured via UV-Visible spectrophotometry. Removal efficiency was calculated using Equation (7):

$$E\ \% = \ [\ (C_o - C_1)/C_o] \quad (7)$$

where C_0 = initial concentration, C_1 = residual concentration after adsorption.

2.7. Kinetics Studies

2.7.1. Pseudo-First-Order Kinetics

This model assumes the rate of occupation of adsorption sites is proportional to unoccupied sites:

$$log(q_e - q_t) = log\ q_e - \left(\frac{k_1}{2.303}\right)t \quad (8)$$

where q_e = equilibrium adsorption capacity, qt = adsorption at time t, k_1 = rate constant.

A graph of $log(q_e - q_{t)}$ versus time t yields a straight line. The slope and intercept of this line are used to determine the values of k_1 and q_e.

2.7.2. Pseudo-Second-Order Kinetics

Assumes chemisorption as the rate-limiting step:

$$\frac{1}{q_t} = \frac{1}{k_2 {q_e}^2} + \left(\frac{1}{q_e}\right) t \qquad (9)$$

where k_2 = rate constant of pseudo-second-order adsorption.

A plot of $\frac{1}{q_t}$ against t gives a linear relationship, from which k_2 and q_e are obtained from the intercept and slope, respectively.

2.8. Adsorption Thermodynamics

Thermodynamic parameters ΔG°, ΔH°, and ΔS° were calculated using Van't Hoff relations. based on equilibrium data obtained at different temperatures. The spontaneity and energy changes associated with the adsorption process were evaluated accordingly.

$$\Delta G^0 = \Delta H^0 - T\Delta S^0 \qquad (12);\ ln\, k_c = \frac{\Delta s}{R} - \frac{\Delta H}{R} \qquad (10)$$

where R = 8.314 J/mol·K, T = temperature (K), k_c = equilibrium constant.

The equilibrium constant (K_C) was calculated as:

$$k_c = \frac{q_e}{c_e} \qquad (11)$$

q_e = amount of adsorbate adsorbed at equilibrium (mg/L); c_e= equilibrium concentration of the unadsorbed metal ions in solution (mg/L). A plot of $ln\, k_c$ versus $\frac{1}{T}$ yields a straight line. The slope and intercept of this plot are used to determine the enthalpy (ΔH°) and entropy (ΔS°) changes associated with the adsorption process.

2.9. Reusability and Regeneration Study

Regeneration was performed using 0.1 M HNO_3, distilled water, and 0.1 M NaOH [7]. The adsorbent underwent three regeneration cycles, with desorption efficiency calculated as:

$$\text{Desorption } (\%) = \frac{\text{amount of } Cu^{2+} \text{ and } Zn^{2+} \text{ desorbed}}{\text{amount of } Cu^{2+} \text{ and } Zn^{2+} \text{ adsorbed}} \times 100 \qquad (12)$$

3. Results and Discussion

3.1. Physicochemical Characterization of Raw and Activated PKS-AC

Table 1 presents proximate compositions. Moisture content decreased from 12.6% to 8.3% after activation. This is expected due to the thermal treatment, which removes bound and free water within the biomass. The reduction suggests significant dehydration during thermal treatment. Moisture content in adsorbents enhances their handling, storage stability, and adsorption efficiency [13]. A lower moisture content prevents pore blockage by water molecules, thereby improving adsorption efficiency, while excessive moisture may limit the quantity of exposed surface sites facilitating adsorption [23]. Ash content increased from 6.5% to 8.5%, signifying a higher concentration of residual inorganic matter post-carbonization. The presence of ash influences the chemical stability and reactivity of the adsorbent. While moderate ash content enhances surface properties and introduces functional groups beneficial for adsorption, excessively high ash content can reduce pore volume and limit adsorption

capacity [25]). The sharp decrease in volatile matter in PKS-AC (from 64.3% to 14.0%) indicates the efficient removal of volatile organic compounds (VOCs) during activation. This reduction in volatile matter contributes to an enhanced carbon structure and higher purity, which is vital for adsorption efficiency. A significant increase in fixed carbon in PKS-AC (from 16.6% to 69.2%) confirms the successful conversion of PKS into highly porous activated carbon. Adsorbents that have higher fixed carbon content show greater adsorption potential owing to their increased surface area and well-developed porosity [16]. The increase in carbon content improves the adsorbent's ability to absorb pollutants through physical and chemical interactions, making PKS-AC suitable for wastewater treatment applications [4]. Bulk density measured at 0.50 g/cm³ implies the material has moderate packing efficiency, suitable for aqueous-phase applications.

Table 1. *Proximate and bulk characteristics of PKS-AC* Physico-chemical Characteristics of Raw PKS and PKS-AC

Parameter (%)	Raw PKS	PKS-AC
Moisture content	12.6	8.30
Ash content	6.50	8.50
Volatile matter	64.3	14.0
Fixed Carbon	16.6	69.20
Bulk density (g/cm^3)	0.8165	0.8365
Yield (%)	-	73.9

3.2. Initial Metal Ion Levels in Industrial Effluent

Heavy metals in untreated paint effluent were quantified using Atomic Absorption Spectrometry (AAS). Table 2 shows copper (Cu) had the highest concentration, followed by manganese (Mn), while cadmium (Cd) was least abundant. Effluent pH was mildly acidic (6.2), typical for industrial paint wastes that contain pigments, solvents, and metallic additives.

Table 2. Heavy Metal Concentration of the Untreated Paint Effluent

Sample	Cu	Zn	Ni	Fe	Ag	Hg	Pb	Cd	Cr	Mn
UWE (mg/L)	15.07	2.16	4.75	8.29	5.02	0.08	6.00	5.09	5.00	10.31

*UWE- Untreated Waste Effluent

3.3. FTIR Spectral Analysis of Surface Functional Groups

The surface chemistry of the PKS-derived activated carbon was examined using Fourier Transform Infrared (FTIR) spectroscopy to identify the functional groups responsible for metal ion adsorption. The spectra, shown in Fig. 1a and b, reveal shifts in characteristic peaks that confirm functional group involvement in adsorption.

The FTIR spectrum before adsorption (Fig. 1a) exhibited absorption peaks at 3414.12 cm^{-1}, associated with O–H stretching vibrations typically attributed to hydroxyl functional groups. Bands at 2920.32 and 2851.12 cm^{-1} represent C–H stretching of aliphatic structures. A strong peak at 1697.41 cm^{-1} is indicative of C=O stretching from carbonyl groups. Other peaks include 1579.97 cm^{-1} (aromatic C=C), 1415.80 and 1354.07 cm^{-1} (phenolic and CH_3 deformation), and 1107.18 cm^{-1} (C–O stretch). Fingerprint region peaks at 875.71, 798.66, and 524.86 cm^{-1} reflect aromatic C–H and skeletal vibrations. After adsorption (Fig. 1b), shifts and changes in intensity were observed. The O–H peak shifted slightly to 3417.98 cm^{-1}, indicating hydrogen bonding or ion exchange. The aliphatic C–H band shifted to 2916.47 cm^{-1} with reduced intensity. The C=O peak remained at 1697.41 cm^{-1} but showed

diminished intensity, suggesting coordination with metal ions. A notable shift of the ether group(C–O) from 1107.18 to 1087.89 cm^{-1} suggests ligand–metal interactions. New peaks at 689.25, 631.95, and 578.66 cm^{-1} indicate the formation of metal–oxygen (M–O) bonds. Table 3 presents a comparison of functional group shifts and their adsorption roles. These changes confirm that hydroxyl, carbonyl, and ether groups facilitated Cu^{2+} and Zn^{2+} binding via complexation, ion exchange, and chelation mechanisms [25].

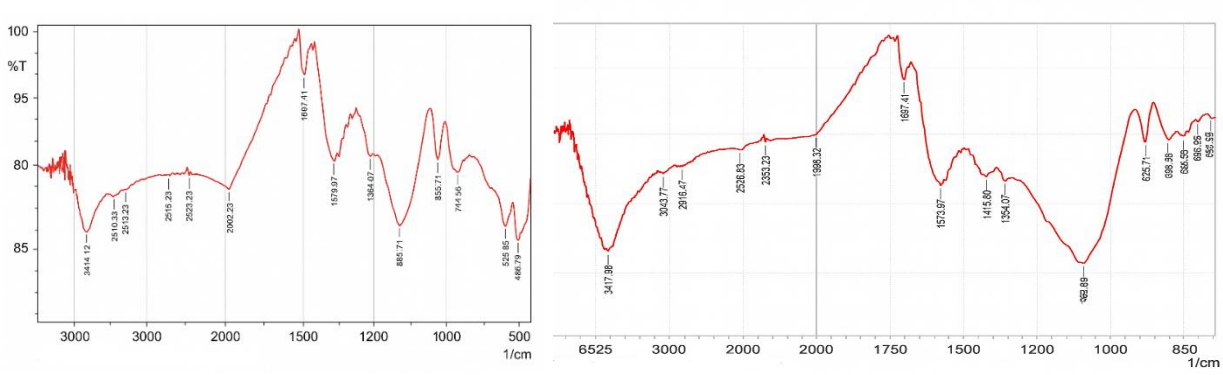

a **b**

Figure 1a and b. FTIR spectrum of PKS-AC before and after adsorption

Table 3. Comparison of FTIR Bands Before and After Adsorption

Functional Group	Wavenumber Before (cm^{-1})	Wavenumber After (cm^{-1})	Interpretation
Hydroxyl (O–H) stretching vibration	3414.12	3417.98	Shifted; hydrogen bonding or exchange
Alkyl (C–H) bond stretching	2920.32, 2851.12	2916.47	Reduced intensity; slight rearrangement
Carbonyl (C=O) group stretching	1697.41	1697.41	Intensity decrease; complexation
Aromatic ring C=C	1579.97	1573.97	Slight shift; minimal involvement
Phenolic/Carboxylic group	1415.80, 1354.07	Same	Reduced intensity; active in binding
Ether or alcohol (C–O) bond stretching	1107.18	1087.89	Shifted; ligand exchange/complexation
New M–O bands	—	689.25, 631.95, 578.66	New peaks; metal–oxygen bond formation

3.4. Standard Curve for Copper and Zinc Ions

To determine metal ion concentrations in the effluent, calibration curves were developed using standard solutions of copper (Cu^{2+}) and zinc (Zn^{2+}) at varying concentrations (50, 100, 150, 200, and 250 mg/L). The absorbance of each solution was measured using a UV-Vis spectrophotometer, and standard curves were plotted. as illustrated in Figure. 2. The resulting linear regressions demonstrated strong correlations between absorbance and concentration, with coefficients of determination (R^2) of

0.9432 for Cu^{2+} and 0.9742 for Zn^{2+}, confirming a reliable fit to the calibration equations (Equations 15 and16).

$$y = 0.003x + 0.4122 \quad (15)$$

$$y = 0.0038x + 0.1287 \quad (16)$$

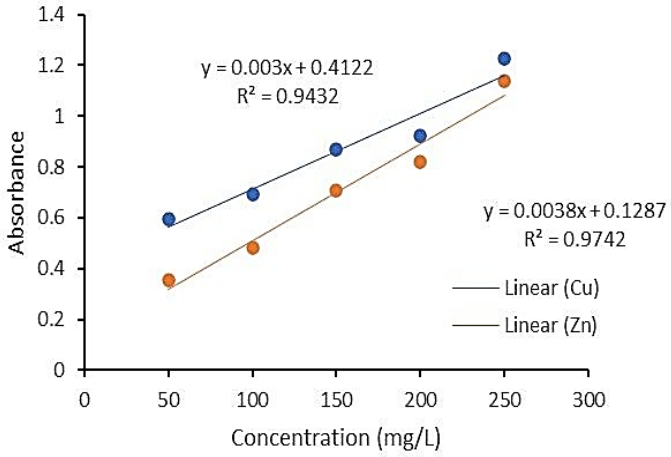

Figure 2. Standard Calibration Curves for Copper and Zinc ions

3.5. Batch Adsorption Studies

The impact of varying the initial effluent pH, contact time, adsorbent dose and temperature on metal ion removal is presented in Figures 3 through 6.

3.5.1. Influence of pH

pH plays a crucial role in determining the adsorption efficiency, as it influences both the ionization state of functional groups on the adsorbent surface and the speciation of metal ions in solution. As shown in Figure 3, the adsorption of Cu^{2+} and Zn^{2+} onto PKS-AC increased progressively with pH, reaching maximum uptake at pH 6. At lower pH (2–3), the removal efficiency was significantly reduced. This can be attributed to the high concentration of protons (H^+) competing with metal cations for active binding sites, thereby limiting the availability of functional groups for Cu^{2+} and Zn^{2+} coordination [13]. In addition, at highly acidic conditions, the surface of PKS-AC is positively charged due to protonation, resulting in electrostatic repulsion between the surface and metal ions [2].

As pH increased beyond 4, proton competition decreased, allowing more negatively charged functional groups such as –OH, –COOH, and –C–O– to interact with the metal ions. The highest removal was observed at pH 6, consistent with previous studies reporting optimal heavy metal uptake by lignocellulosic-based activated carbons within a pH range of 5–7 [28,29]. Beyond pH 6, a slight decline in adsorption was observed, likely due to the hydrolysis and precipitation of Cu^{2+} and Zn^{2+} as hydroxide species, which reduces their availability for adsorption [15, 30].

This behaviour suggests that electrostatic attraction and surface complexation were the dominant mechanisms of adsorption, and that PKS-AC is most effective under near-neutral conditions. Such conditions are particularly relevant for real wastewater treatment since many industrial effluents, including those from paint manufacturing, fall within this pH range after minimal pretreatment.

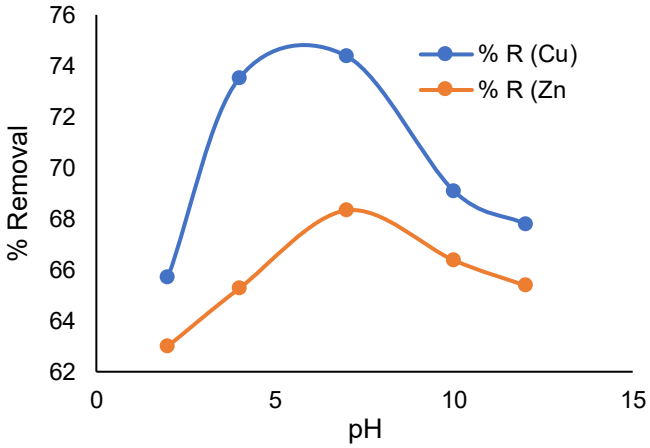

Figure 3. Effect of pH on % removal of Cu^{2+} and Zn^{2+}

3.5.2. Effect of Adsorbent Dosage (g/L)

Adsorbent dosage is a critical factor in the adsorption process, as it directly influences the number of available active sites for metal ion uptake. As presented in Figure 4, the removal efficiency of Cu^{2+} and Zn^{2+} increased with an increase in PKS-AC dosage from 0.2 to 1.0 g/100 mL. This trend is expected because higher dosages provide a greater number of active functional groups and adsorption sites, thereby enhancing metal ion sequestration [31]. At 1.0 g/100 mL, the maximum removal efficiencies were achieved, indicating near-saturation of available binding sites relative to the metal ion concentration in solution.

However, when the dosage exceeded 1.0 g/100 mL, the increase in removal efficiency was minimal, suggesting that equilibrium between solute concentration and available active sites had been reached. A similar saturation effect has been reported in studies utilizing agricultural waste-derived activated carbons for heavy metal removal [31,32]. Additionally, at higher dosages, particle aggregation and overlapping of adsorption sites may occur, which reduces the effective surface area and prevents full utilization of the adsorbent [28].

Generally, an increase in adsorbent dosage leads to greater adsorption efficiency. This improvement is attributed to the greater number of accessible binding sites at higher adsorbent concentrations. However, once the optimal dosage is exceeded, the removal efficiency levels off, likely as a result of site saturation, as previously observed by Kuwer et al. [14] and Gajera et al. [27].

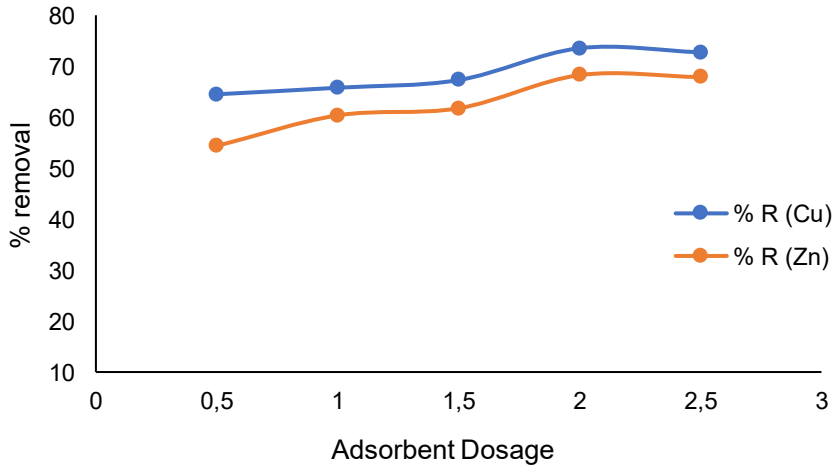

Figure 4. Effect of Dosage on % removal of Cu^{2+} and Zn^{2+}

3.5.3. Effect of Contact Time

The duration of interaction between adsorbent and adsorbate is a critical parameter in adsorption processes, as it determines the rate and extent of equilibrium attainment. As shown in Figure 5, the removal efficiency of Cu^{2+} and Zn^{2+} ions increased rapidly within the first 30 minutes, followed by a gradual rise until equilibrium was reached at around 90 minutes. Beyond this point, no significant increase in removal was observed, suggesting that the active sites on the PKS-AC surface were nearly saturated.

The initial rapid phase of adsorption can be attributed to the abundant availability of vacant active sites and strong electrostatic attraction between metal ions and surface functional groups such as hydroxyl and carbonyl groups, as confirmed by FTIR analysis. The subsequent slower phase is due to intraparticle diffusion resistance and decreased availability of free sites as metal ions occupy them [33]. This biphasic behaviour aligns with findings from similar studies employing agricultural byproduct-derived activated carbons for heavy metal removal [34,35]. The attainment of equilibrium within 90 minutes demonstrates the efficiency of PKS-AC, making it suitable for practical wastewater treatment applications where shorter treatment times are preferred.

Kinetic modelling further confirmed that the adsorption process followed a pseudo-second-order kinetic model, indicating that chemisorption involving valence forces or electron sharing was the rate-limiting step rather than mass transfer alone [36].

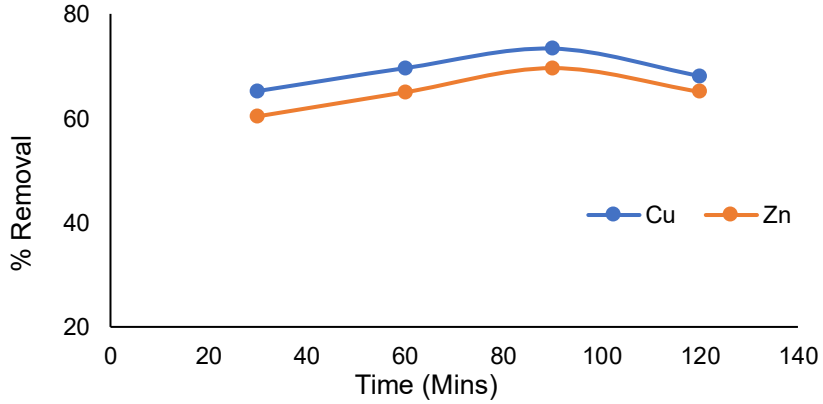

Figure 5. Effect of Time on % removal of Cu^{2+} and Zn^{2+}

3.5.4. Effect of Temperature

The influence of temperature on the adsorption capacity was examined at four different levels: 25°C, 35°C, 45°C, and 5°C as shown in Figure 6. At 25°C, the removal efficiencies for Cu^{2+} (75.0%) and Zn^{2+} (78.5%) were nearly identical. A slight increase in adsorption was observed at 35°C for both Cu^{2+} (70.0%) and Zn^{2+} (74.0%). As the temperature increased further, Cu adsorption declined significantly, while Zn adsorption exhibited a moderate decrease. At 45°C, Cu^{2+} adsorption dropped to 59.76%, whereas Zn adsorption declined slightly to 70.5%. At 55°C, Cu^{2+} adsorption further decreased to 49.73%, while Zn adsorption slightly decreased to 68.0%. The sharper decline in Cu^{2+} adsorption beyond 45°C implies that the adsorption for Cu^{2+} is exothermic, indicating that the process is more efficient at lower temperatures. In contrast, Zn adsorption followed a similar trend but at a slower rate, indicating a relatively lower sensitivity to temperature variations. At higher temperatures, the decreased adsorption efficiency can be attributed to increased molecular motion, which may lead to desorption of previously adsorbed ions or reduced electrostatic attractions between the metal cations and functional groups on the adsorbent surface. While Cu^{2+} adsorption is more affected by temperature, Zn adsorption remains relatively stable, suggesting a stronger affinity of PKS-AC for Zn ions at elevated temperatures [16], [24].

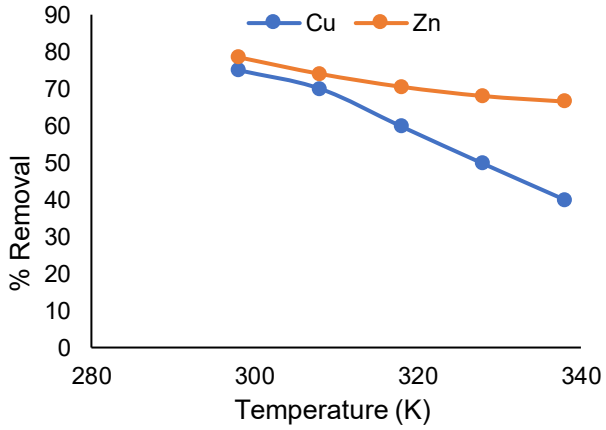

Figure 6. Effects of Temperature on % removal of Cu^{2+} and Zn^{2+}

3.6. Adsorption Kinetics studies

Figures 7 and 8 shows the time-dependent adsorption data onto PKS-AC using pseudo-first-order and pseudo-second-order kinetic models. The logarithmic plots of $\log(q_e - q_t)$ against time for Cu^{2+} and Zn^{2+} exhibit a linear decrease, suggesting that their adsorption follows a pseudo-first-order kinetic model. However, the linear nature of the pseudo-second-order plot indicates a better fit for both metals, with correlation coefficients (R^2) exceeding 0.99, as shown in Table 4. Additionally, the equilibrium adsorption capacities (q_e) closely match the experimental values, further validating the model's applicability. This suggests that the adsorption mechanism indicates that the process is likely governed by chemisorption, involving electron sharing or exchange between the adsorbent surface and the metal ions, as described by Rubai et al. [17]. Comparable findings have been reported by Baby and Hussein [2] and Baby [6] where the pseudo-second-order model effectively described similar adsorption systems. These results imply that the rate-limiting step involves specific interactions between the functional groups on the PKS-AC surface and the adsorbate species.

Table 4. Comparison of kinetic parameters for Cu^{2+} and Zn^{2+} adsorption on PKS-AC

Kinetic models	Parameters	Cu
Pseudo-first order	$q_{e,calc}$(mg/g)	1.982
	$q_{e,exp}$ (mg/g)	5.11
	K_1 (min^{-1})	0.0226
	R^2	0.7394
	RMSE	1.909
Pseudo-second order	$q_{e,calc}$ (mg/g)	5.72
	$q_{e,exp}$ (mg/g)	5.11
	K_2 (min^{-1})	0.0278
	R^2	0.9936
	RMSE	0.307

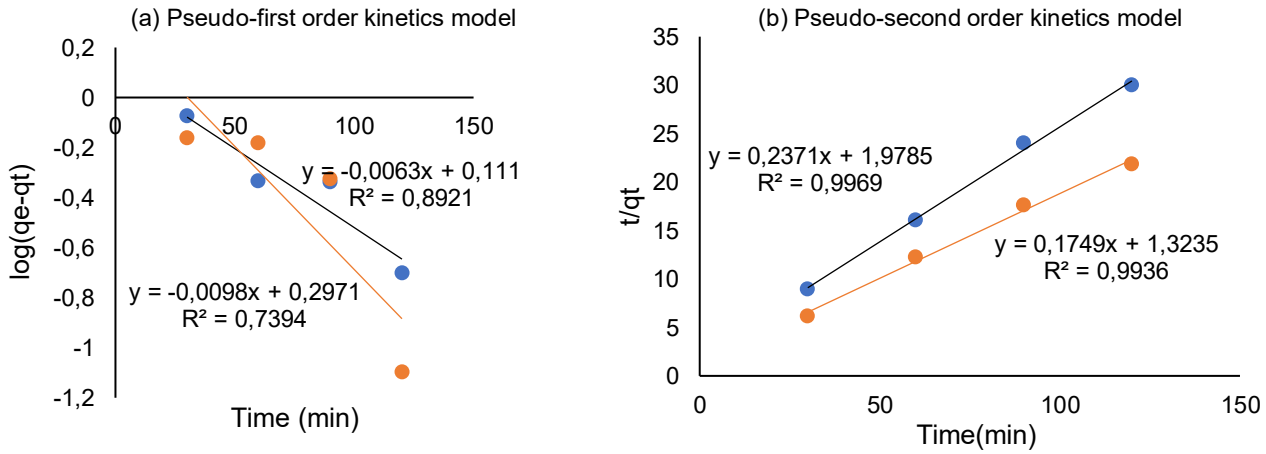

Figure. 7a and b. Kinetic Plot for Cu and Zn Removal onto PKS-AC for Pseudo First and Second order

3.7. Thermodynamics Studies

Thermodynamic parameters (ΔG°, ΔH°, ΔS°) were evaluated to assess the spontaneity and feasibility of adsorption. As shown in Table 5, ΔG° values were negative at all studied temperatures, confirming that adsorption of both Cu^{2+} and Zn^{2+} onto PKS-AC was spontaneous. The magnitude of ΔG° became more negative with increasing temperature, indicating improved adsorption feasibility at higher temperatures.

Moreover, the positive enthalpy change (ΔH) values for both Cu^{2+} and Zn^{2+} indicate that the adsorption process is endothermic, meaning that increased temperature enhances adsorption efficiency. The positive entropy (ΔS°) values suggest increased randomness at the solid–solution interface, likely due to structural rearrangements on the adsorbent surface during metal ion binding. Collectively, these findings confirm that the adsorption of Cu^{2+} and Zn^{2+} onto PKS-AC is spontaneous, endothermic, and entropy-driven [4], [16].

Table 5. Thermodynamic parameters for Cu^{2+} and Zn^{2+} adsorption on PKS-AC

Metal	ΔH (KJ/ mol)	ΔS (KJ/ mol K	ΔG (KJ/mol)				
			298K	308K	318K	328K	338
Cu	0.321	0.062	-1.815	-1.878	-1.940	-2.002	-2.064
Zn	0.126	0.003625	-1.0816	-1.1179	-1.1542	-1.1905	-1.2268

3.8. Regeneration and Reusability Study of Spent PKS-AC

PKS-AC retained its adsorption capacity across three cycles, with minimal reductions of 0.5%, 2.2%, and 2.5% for distilled water, HNO_3, and NaOH washings, respectively. These results confirm that PKS-AC is an effective and reusable adsorbent, maintaining significant adsorption efficiency over multiple cycles confirming its practical reusability in wastewater treatment applications [7].

Table 6. Regeneration efficiencies of PKS-AC after three cycles

Regeneration cycle	Removal efficiency (%)			Removal efficiency (%)		
	Distilled water	HNO_3	NaOH	Distilled water	HNO_3	NaOH
1st cycle	70.00	67.50	73.00	63.90	65.30	70.00
3rd cycle	69.50	64.30	70.5	62.80	64.10	68.50

4. Conclusion

This study demonstrated that palm kernel shell-derived activated carbon (PKS-AC) is an efficient and sustainable adsorbent for the removal of Cu^{2+} and Zn^{2+} from real industrial paint effluent. The adsorption process was best described by the pseudo-second-order kinetic model, confirming chemisorption, while thermodynamic analysis revealed that the process is both spontaneous and endothermic. FTIR analysis verified the role of surface functional groups in metal binding, and regeneration experiments confirmed that PKS-AC retains its adsorption capacity across multiple cycles, highlighting its reusability. The novelty of this work lies in applying a low-cost, agricultural byproduct to treat actual paint wastewater, moving beyond studies limited to synthetic effluents. By integrating performance evaluation with kinetic, thermodynamic, and reusability analyses, this research provides a holistic demonstration of PKS-AC's potential for real-world application. These findings support the use of PKS-AC in sustainable wastewater treatment systems.

Conflict of Interest: The authors declare that there are no conflicts of interest.

5. References

[1] A. Azimi, A. Azari, M. Rezakazemi, and M. Ansarpour, "Removal of heavy metals from industrial wastewaters: A review," *ChemBioEng Reviews*, vol. 4, no. 1, pp. 37–59, 2017, doi: 10.1002/cben.201600010.

[2] R. Baby and M. Z. Hussein, "Application of palm kernel shell as bio adsorbent for the treatment of heavy metal contaminated water," *Int. J. Adv. Sci. Eng. Technol.*, vol. 1, no. 1, pp. 10–16, 2019.

[3] G. L. Ndagire and R. B. Kalengyo, "Coagulation and filtration combined to treat paint factory wastewater: Empirical insights from Uganda," presented at the *Int. Conf. Recent Trends Environ. Sci. Eng.*, Canada, Jun. 2023.

[4] M. O. Aremu, A. O. Arinkoola, I. A. Olowonyo, and K. K. Salam, "Improved phenol sequestration from aqueous solution using silver nanoparticle modified palm kernel shell activated carbon," *Heliyon*, vol. 6, e04492, 2020, doi: 10.1016/j.heliyon.2020.e04492.

[5] T. E. Oladimeji, B. O. Odunoye, F. B. Elehinafe, O. R. Obanla, and O. A. Odunlami, "Production of activated carbon from sawdust and its efficiency in the treatment of sewage water," *Heliyon*, vol. 7, no. 1, 2021.

[6] R. Baby, "Ecofriendly approach for treatment of heavy-metal-contaminated water using activated carbon of kernel shell of oil palm," 2020.

[7] M. A. Abdel-Khalek, M. K. Abdel Rahman, and A. A. Francis, "Experimental design and desirability analysis for optimizing the bio-sorption of liquid paint-related wastes onto solid eggshell wastes," *Environmental Processes*, vol. 7, pp. 493–508, 2020, doi: 10.1007/s40710-020-00435-6.

[8] O. A. Ekpete, A. C. Marcus, and V. Osi, "Preparation and characterization of activated carbon obtained from plantain (Musa paradisiaca) fruit stem," 2017, doi: 10.1155/2017/8635615.

[9] E. H. Ezechi, S. R. B. M. Kutty, A. Malakahmad, and M. H. Isa, "Characterization and optimization of effluent dye removal using a new low-cost adsorbent: Equilibrium, kinetics and thermodynamic study," *J. Chem. Soc. Nigeria*, vol. 47, no. 6, pp. 1335–1347, 2022.

[10] C. Anyika, N. A. M. Asri, Z. A. Majid, A. Yahya, and J. Jaafar, “Synthesis and characterization of magnetic activated carbon developed from palm kernel shells,” *Nanotechnol. Environ. Eng.*, vol. 2, p. 16, 2017, doi: 10.1007/s41204-017-0027-6.

[11] R. F. Abdullah, U. Rashid, Y. H. Taufiq-Yap, M. L. Ibrahim, C. Ngamcharussrivichai, and M. Azam, “Synthesis of bifunctional nano catalyst from waste palm kernel shell and its application for biodiesel production,” *RSC Advances*, vol. 10, pp. 27183–27193, 2020, doi: 10.1039/d0ra04306k.

[12] D. Prahas, Y. Kartika, N. Indraswati, and S. Ismadji, “Activated carbon from jackfruit peel waste by H_3PO_4 chemical activation: Pore structure and surface chemistry characterization,” *Chem. Eng. J.*, vol. 140, pp. 32–42, 2008.

[13] V. I. Onwukeme and C. C. Egemba, “Removal of silver and cadmium from industrial waste water using chemically modified palm kernel shells,” *J. Chem. Soc. Nigeria*, vol. 47, no. 6, pp. 1335–1347, 2022.

[14] P. Kuwer, A. Yadav, and P. K. Labhasetwar, “Adsorption of cupric, cadmium and cobalt ions from the aqueous stream using the composite of iron (II, III) oxide and zeolitic imidazole framework-8,” *Water Sci. Technol.*, vol. 84, no. 9, pp. 2288–2303, 2021, doi: 10.2166/wst.2021.452.

[15] R. Hotagamuge et al., “Copper modified activated bamboo charcoal to enhance adsorption of heavy metals from industrial wastewater,” *Environ. Nanotechnol. Monit. Manage.*, vol. 16, p. 100562, 2021.

[16] N. K. Soliman and A. F. Moustafa, “Industrial solid waste for heavy metals adsorption features and challenges: A review,” *J. Mater. Res. Technol.*, vol. 9, no. 5, pp. 10235–10253, 2020.

[17] H. Rubai, A. K. H. Al-Dahan, and B. A. Jasim, “Green synthesis of iron oxide nanoparticles and their modification with CTAB for the decolorization of dye reactive blue 238,” *Iraqi J. Sci.*, vol. 64, no. 4, pp. 1592–1600, 2023, doi: 10.24996/ijs.2023.64.4.2.

[18] M. G. Ghoniem, M. A. Ben Aissa, F. A. M. Ali, and M. Khairy, “Efficient and rapid removal of Pb(II) and Cu(II) heavy metals from aqueous solutions by MgO nanorods,” *Inorganics*, vol. 10, no. 12, pp. 1–17, 2022.

[19] Blanco, M. L. Pignata, H. R. Lascano, M. J. Salazar, and J. H. Rodriguez, “Lead uptake and translocation pathways in soybean seedlings: The role of ion competition and transpiration rates,” *Environ. Sci. Pollut. Res.*, vol. 28, no. 16, pp. 20624–20636, 2021.

[20] H. Langergren and B. Svenska, “Zur Theorie der sogenannten Adsorption geloester Stoffe,” *Veternskapsakad. Handlingar*, vol. 24, pp. 1–39, 1898.

[21] G. Latinwo, “Removal of phenol from paint wastewater by adsorption onto phosphoric acid activated carbon produced from coconut shell: Isothermal and kinetic modelling studies,” *Chem. Mater. Res.*, 2015.

[22] M. Kavand, P. Eslami, and L. Razeh, “The adsorption of cadmium and lead ions from the synthesis wastewater with the activated carbon: Optimization of the single and binary systems,” *J. Water Process Eng.*, vol. 34, pp. 101–151, 2020.

[23] S. Rastegar, H. Rezaei, and H. Yousefi, “Removal of lead (Pb) from aqueous solutions using lignocellulose nanofiber,” *Arch. J. Environ. Health Eng.*, vol. 8, no. 1, pp. 1–8, 2021, doi: 10.34172/ajehe.2021.01.

[24] Y. Wang, H. Li, and S. Lin, “Advances in the study of heavy metal adsorption from water and soil by modified biochar,” *Water*, vol. 14, 2022.

[25] I. Aubeeluck-Ragoonauth et al., “Physicochemical analysis of wastewater generated from a coating industry in Mauritius,” *Environ. Monit. Assess.*, vol. 194, no. 10, p. 646, 2022.

[26] O. O. E. Onawumi, A. A. Sangoremi, and O. S. Bello, “Preparation and characterization of activated carbon from groundnut and egg shells as viable precursors for adsorption,” *J. Appl. Sci. Environ. Manage.*, vol. 25, no. 9, pp. 1707–1713, 2021.

[27] R. Gajera, R. V. Patel, A. Yadav, and P. K. Labhasetwar, “Adsorption of cationic and anionic dyes on photocatalytic flyash/TiO_2 modified chitosan biopolymer composite,” J. Water Process Eng., vol. 49, p. 102993, 2022, doi: 10.1016/j.jwpe.2022.102993.

[28] Foo, K. Y., and Hameed, B. H. (2010). Insights into the modeling of adsorption isotherm systems. *Chemical Engineering Journal, 156*(1), 2–10.

[29] A. A. Ahmad, B. H. Hameed, and N. Aziz, “Adsorption of direct dye on palm ash: Kinetic and equilibrium modeling,” *J. Hazard. Mater.*, vol. 141, no. 1, pp. 70–76, 2007.

[30] C. A. Igwegbe, O. D. Onukwuli, and C. O. B. Okoye, “Adsorptive removal of heavy metals from aqueous solution using activated carbon from palm kernel shell,” *J. Appl. Sci. Environ. Manage.*, vol. 20, no. 2, pp. 259–272, 2016.

[31] B. H. Hameed, A. L. Ahmad, and K. N. A. Latiff, “Adsorption of basic dye on activated carbon prepared from rattan sawdust,” *Dyes Pigments*, vol. 75, no. 1, pp. 143–149, 2007.

[32] Y. S. Ho and G. McKay, “Pseudo-second order model for sorption processes,” *Process Biochem.*, vol. 34, no. 5, pp. 451–465, 1999.

[33] S. Babel and T. A. Kurniawan, “Low-cost adsorbents for heavy metals uptake from contaminated water: A review,” *J. Hazard. Mater.*, vol. 97, nos. 1–3, pp. 219–243, 2003.

[34] C. A. Igwegbe and O. D. Onukwuli, “Adsorptive removal of Pb^{2+} and Ni^{2+} ions from aqueous solution using activated carbon prepared from palm kernel shell,” *Environ. Nanotechnol. Monit. Manage.*, vol. 9, pp. 128–135, 2018.

[35] A. Ahmad, M. Rafatullah, O. Sulaiman, M. H. Ibrahim, R. Hashim, and N. Ahmad, “Removal of Cu(II) and Pb(II) ions from aqueous solutions by adsorption on sawdust of Meranti wood,” *Desalination*, vol. 247, nos. 1–3, pp. 636–646, 2009.